iScience

CellPress
OPEN ACCESS

Article

Systemic phospho-defective and phospho-mimetic Drp1 mice exhibit normal growth and development with altered anxiety-like behavior

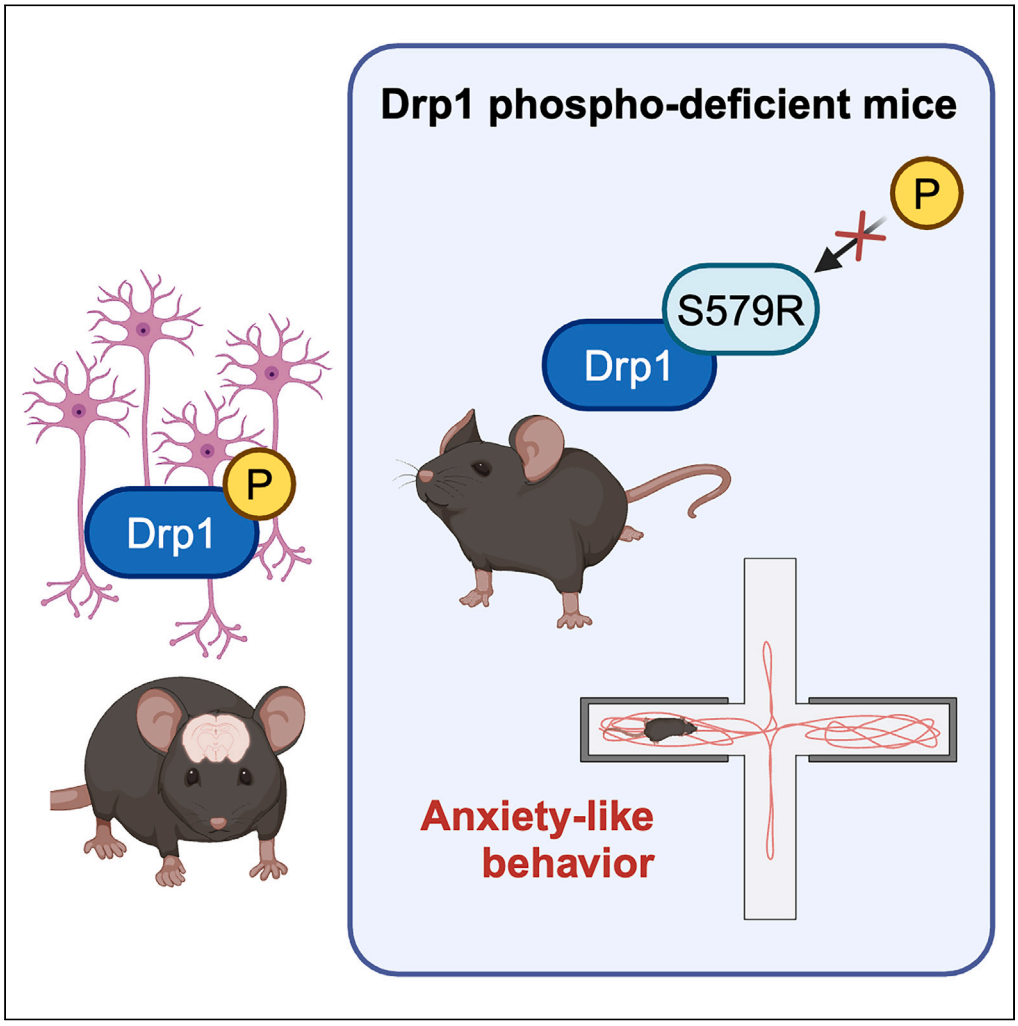

Arisa Ikeda, Miho Iijima, Hiromi Sesaki

miijima@jhmi.edu (M.I.)
hsesaki@jhmi.edu (H.S.)

Highlights

Drp1 is highly phosphorylated at S579 in post-mitotic neurons in mice

Drp1 S579 phosphorylation is dispensable for development and growth in mice

Drp1 S579 phosphorylation influences anxiety behaviors

Drp1 phospho-deficient and phospho-mimetic mice provide useful animal models

Ikeda et al., iScience 27, 109874
June 21, 2024
https://doi.org/10.1016/j.isci.2024.109874

iScience

CellPress
OPEN ACCESS

Article

Systemic phospho-defective and phospho-mimetic Drp1 mice exhibit normal growth and development with altered anxiety-like behavior

Arisa Ikeda,[1] Miho Iijima,[1,*] and Hiromi Sesaki[1,2,*]

SUMMARY

Mitochondrial division controls the size, distribution, and turnover of this essential organelle. A dynamin-related GTPase, Drp1, drives membrane division as a force-generating mechano-chemical enzyme. Drp1 is regulated by multiple mechanisms, including phosphorylation at two primary sites: serine 579 and serine 600. While previous studies in cell culture systems have shown that Drp1 S579 phosphorylation promotes mitochondrial division, its physiological functions remained unclear. Here, we generated phospho-mimetic Drp1 S579D and phospho-defective Drp1 S579R mice using the CRISPR-Cas system. Both mouse models exhibited normal growth, development, and breeding. We found that Drp1 is highly phosphorylated at S579 in brain neurons. Notably, the Drp1 S579D mice showed decreased anxiety-like behaviors, whereas the Drp1 S579R mice displayed increased anxiety-like behaviors. These findings suggest a critical role for Drp1 S579 phosphorylation in brain function. The Drp1 S579D and S579R mice thus offer valuable *in vivo* models for specific analysis of Drp1 S579 phosphorylation.

INTRODUCTION

Mitochondrial division controls their number, size, and connectivity, coordinating with the opposing activity of mitochondrial fusion.[1–3] Defects in mitochondrial division have been linked to various human diseases and conditions, particularly affecting energy-demanding tissues such as the brain and heart.[4–8] Mitochondrial division is also crucial for remodeling energy metabolism in tumorigenesis.[7,9] Drp1, a member of the dynamin family, plays a vital role in mitochondrial division as a force-generating mechano-chemical GTPase. Drp1 is a cytosolic soluble protein that is recruited to the mitochondrial outer membrane through interactions with receptor proteins such as Mff, MiD49, MiD51, and Fis1.[10] Additionally, the actin cytoskeleton formed on mitochondria enhances Drp1's mitochondrial localization.[11] On the outer membrane, Drp1 oligomerizes into spiral filaments and wraps around mitochondria. The force driving membrane scission is generated by conformational changes in the Drp1 filaments, stimulated by GTP hydrolysis.[12] This key step is facilitated by multiple mechanisms, including its oligomerization, as well as interaction with the receptors, the actin cytoskeleton, and the mitochondria-specific phospholipid cardiolipin.[1,2,11,12] In contrast, association with another phospholipid, phosphatidic acid, suppresses Drp1's function on the outer membrane.[1,2,13]

Drp1 undergoes phosphorylation at two primary sites. In the mouse Drp1 (isoform 3, most widely expressed[14,15]), phosphorylation occurs at serine 579 (S579), located in its unstructured variable domain, and serine 600 (S600), situated in the stalk domain that mediates both intra- and intermolecular interactions[16,17] (Figures 1A and 1B). In human Drp1 (isoform 1), the corresponding serine residues are serine 616 and serine 637[16,17] (Figures 1A and 1B). Hereafter, we use the mouse Drp1 nomenclature. Phosphorylation at S579 has been shown to predominantly promote mitochondrial division, while S600 phosphorylation exhibits both inhibitory and stimulatory roles.[18–32] Interestingly, a recent biochemical study using purified Drp1 revealed that S579 phosphorylation does not enhance Drp1's activity but rather suppresses its activation by actin, receptors, and cardiolipin.[33] It has been proposed that the regulatory mechanism of mitochondrial division via S579 phosphorylation may involve isoform-specific effects, as Drp1 generates various isoforms in different cell types and tissues,[14,15,34] and other factors such as nucleoside diphosphate kinases, which could supply GTP to dynamin and dynamin-related GTPase family proteins.[33,35–37] Moreover, this phosphorylation might coordinate and orchestrate these multiple regulatory processes with other post-translational signaling mechanisms of Drp1, such as ubiquitination, SUMOylation, O-GlcNAcylation, and S-nitrosylation.[16]

S579 phosphorylation of Drp1 occurs in various cellular contexts, optimizing mitochondrial size, cell death, and energy production by orchestrating mitochondrial dynamics and cellular activities. During mitosis in cultured cell lines, for example, Cdk1/cyclin B phosphorylates Drp1 at S579, a process further regulated by the small Ras-like GTPase RALA and its effector RALBP1.[38,39] This phosphorylation promotes mitochondrial division, leading to the creation of many small mitochondria, which facilitates equal mitochondrial inheritance in daughter cells.[38,39] Additionally, S579 phosphorylation by Erk2, crucial in KRAS-driven transformation and tumorigenesis, remodels energy metabolism

[1]Department of Cell Biology, Johns Hopkins University School of Medicine, Baltimore, MD 21212, USA
[2]Lead contact
*Correspondence: miijima@jhmi.edu (M.I.), hsesaki@jhmi.edu (H.S.)
https://doi.org/10.1016/j.isci.2024.109874

A

	UniProt ID	Length	Alternative exon	Phosphorylation 1st	Phosphorylation 2nd
Mouse isoform3 (short isoform)	Q8K1M6-3	699 aa	-	Ser579	Ser600
Human isoform1	O00429-1	736 aa	+ C, D	Ser616	Ser637

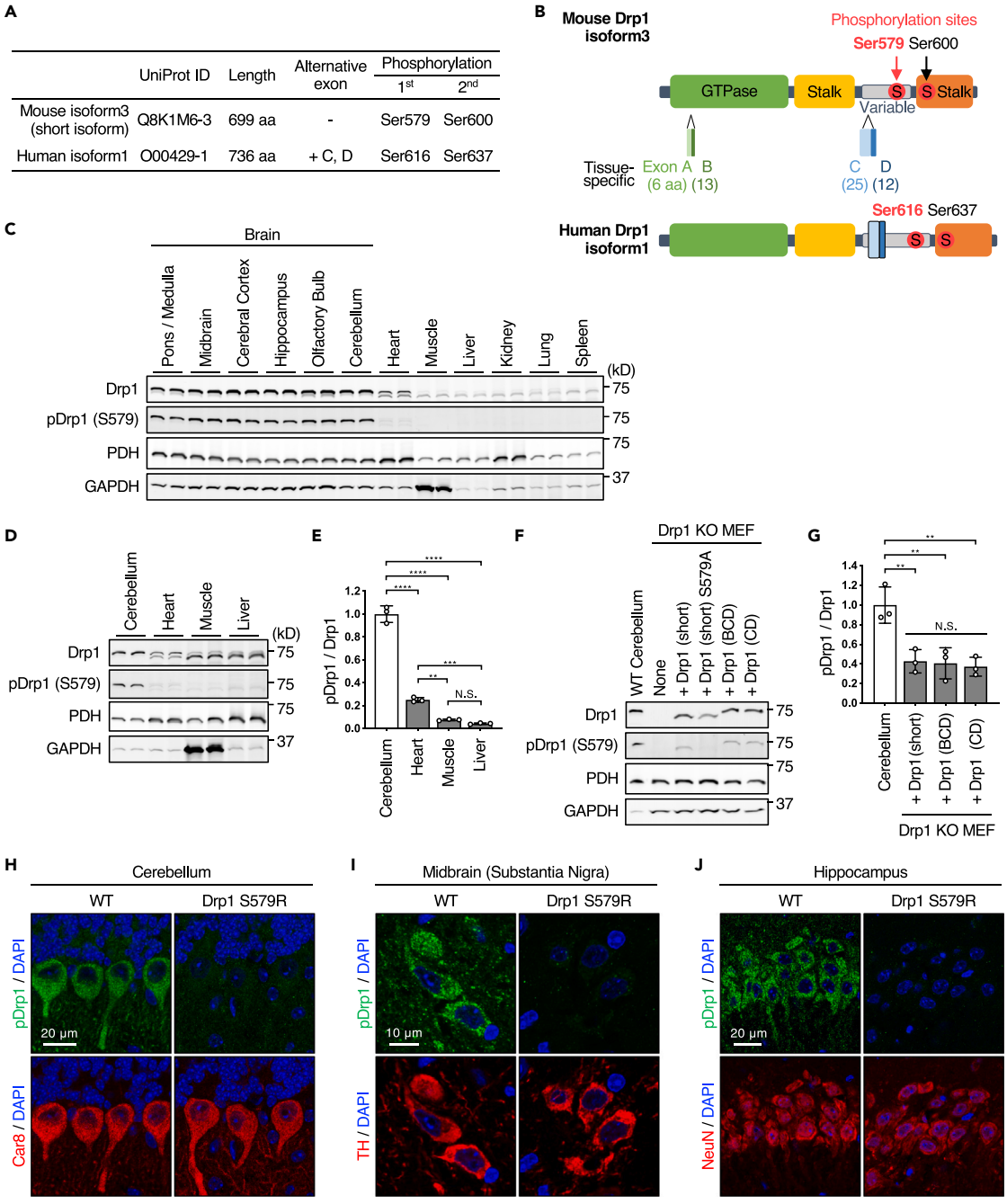

Figure 1. Drp1 S579 is strongly phosphorylated in neurons

(A) A table shows the UniProt ID, amino acid length, alternative exons, and phosphorylation sites of mouse Drp1 (isoform 3, the most widely expressed)[14,15] and human Drp1 (canonical isoform 1).

(B) The domain architecture of mouse and human Drp1 is depicted. The two conserved phosphorylation sites, located in the variable domain, are S579 and S600 for mouse Drp1, and S616 and S637 for human Drp1. The four alternative exons are also shown (A–D).

(C) Mouse tissues and brain subregions were analyzed by western blotting using antibodies to Drp1, pDrp1 (S579), the mitochondrial protein PDH, and GAPDH. A total of 10 μg of protein was loaded per lane.

(D) Western blotting of the indicated mouse tissues was performed, loading 10 μg of protein for the cerebellum, while the loading amounts for the heart, muscle, and liver were adjusted to equalize the Drp1 band intensities across these tissues.

(E) The ratios of pDrp1 to Drp1 were quantified and normalized relative to that of the cerebellum. Bars represent means ± SD (n = 3).

(F) Drp1-KO MEFs transduced with lentiviruses carrying different Drp1 isoforms, such as Drp1 short, phospho-defective Drp1 short (S579A), Drp1 BCD, or Drp1 CD, were subjected to western blotting alongside the cerebellum of WT mice.

Figure 1. *Continued*

(G) The pDrp1/Drp1 ratios of the three isoforms were quantified relative to that of the cerebellum. Bars represent means ± SD (n = 3). Statistical analysis was performed using one-way ANOVA with post hoc Tukey test in (E and G); **$p < 0.01$, ***$p < 0.001$, ****$p < 0.0001$.

(H–J) Immunofluorescence microscopy of the cerebellum (H), the substantia nigra (I), and hippocampal CA2 region (J) in WT and Drp1 S579R mice. 7 μm frozen sections were cut and stained with antibodies to pDrp1 (S579) together with the Purkinje neuron marker Car8 (H), the dopaminergic neuron marker tyrosine hydroxylase (TH) (I), and the post-mitotic neuron marker NeuN (J).

and ensures effective mitochondrial inheritance in dividing cancer cells.[40,41] Similarly, during the reprogramming of mouse embryonic fibroblasts (MEFs) to pluripotent stem cells, and in hypoxia-induced mitochondrial division, Erk1/2 mediates S579 phosphorylation.[42,43] In an Alzheimer's disease model using cultured mouse neurons, Cdk5 phosphorylates Drp1 at S579 to stimulate mitochondrial division, a mechanism also linked to cell death induced by NMDA.[44] Moreover, RIPK1 phosphorylates Drp1 at S579 upon swine influenza virus infection, activating the NLRP3 inflammasome.[45] These studies collectively highlight the pivotal roles of S579 phosphorylation in mitochondrial division and cellular activities *in vitro*. Given these findings, investigating the physiological role of S579 phosphorylation *in vivo*, particularly in animal models, is both significant and necessary.

The physiological role of Drp1 has been extensively studied in various cell types and tissues, including cardiomyocytes in the heart, hepatocytes in the liver, and neurons in the brain, through the employment of both systemic and conditional knockout (KO) of Drp1 in mice.[1,2] Systemic KO of Drp1 results in embryonic lethality, while cardiomyocyte-specific Drp1-KO mice exhibit cardiac dysfunction and premature death post-birth.[46–49] In the liver, hepatocytes with Drp1 KO lose mitochondrial division activity and exhibit enlarged mitochondria, leading to impaired mitophagy.[50] Furthermore, Drp1 KO in Purkinje and dopaminergic neurons triggers their degeneration, and its KO in hippocampal neurons resulted in bioenergetic deficits and memory defects.[51–53] These findings have highlighted the critical physiological importance of Drp1 *in vivo*. However, the physiological significance of Drp1's S579 phosphorylation *in vivo* has not been thoroughly investigated, primarily due to the lack of suitable model systems. To address this gap, in this study, we utilized the CRISPR-Cas genome editing strategy to generate and characterize two novel mouse models: one with a phospho-defective variant of Drp1 (S579 replaced with arginine, S579R) and another with a phospho-mimetic variant (S579 replaced with aspartic acid, S579D).

RESULTS

Drp1 S579 is highly phosphorylated in the brain

We analyzed the phosphorylation level of Drp1 at S579, denoted as pDrp1(S579), in various mouse tissues using western blotting with the same amounts of proteins loaded per lane (Figures 1A and 1B). Higher levels of pDrp1(S579) were observed in the brain compared to other tissues such as the heart, skeletal muscle, liver, kidney, lung, and spleen (Figure 1C). This strong phosphorylation of Drp1 was noted in all six subregions analyzed: the pons/medulla, midbrain, cerebral cortex, hippocampus, olfactory bulb, and cerebellum. We also observed that the expression levels of Drp1 were higher in the brain and heart (Figure 1C). To accurately compare the ratio of pDrp1(S579) to the total Drp1 level, we adjusted the loading amount to equalize the total Drp1 levels in the cerebellum, heart, muscle, and liver (Figure 1D). Even after this adjustment of Drp1 amounts, the phosphorylation level in the cerebellum was significantly higher than in the other tissues (Figure 1E). The level of pDrp1(S579) in the heart was slightly higher than in the liver and muscle, but markedly lower than in the cerebellum. Therefore, Drp1 S579 is highly phosphorylated in the brain in mice.

Drp1 has four alternative exons, A–D (Figure 1A, 1B, S1A, and S1B), which generate 10 different isoforms in mice.[14,15] Exons A and B are located in the GTPase domain, while exons C and D reside in the variable domain containing the S579 phosphorylation site. To investigate whether the observed differences in S579 phosphorylation levels are due to the expression of different isoforms in various tissues, we compared the S579 phosphorylation levels of three specific isoforms. These include the short isoform (Drp1 short, 699 aa) lacking all four alternative exons, which is ubiquitously expressed in many tissues, and the Drp1 isoforms with exon B, C, and D (Drp1 BCD, 749 aa) and with exons C and D (Drp1 CD, 736 aa), both predominantly found in the brain.[14,15] As a negative control, we used a phospho-defective mutant of the short isoform (S579A). These four isoforms were expressed in Drp1-KO MEFs using a lentivirus and analyzed by western blotting with antibodies specific to Drp1 and pDrp1(S579). The results revealed no significant differences in the S579 phosphorylation levels among these three isoforms expressed in MEFs (Figures 1F and 1G). This suggests that different isoforms can be phosphorylated at similar levels, irrespective of their alternative exon composition.

When comparing the phosphorylation level in these MEFs to that in the cerebellum, we found a stronger S579 phosphorylation signal with equivalent amounts of total Drp1 in the cerebellum (Figures 1F and 1G). Therefore, it seems the brain has more active kinase activities or less phosphatase activities for Drp1 S579 compared to MEFs.

Drp1 S579 is highly phosphorylated in neurons

Given the diversity of cell types in the brain, including neurons and glial cells, we sought to identify the specific cells where Drp1 is phosphorylated at S579. We performed laser confocal immunofluorescence microscopy on frozen sections of the wild-type (WT) mouse brain, using antibodies against pDrp1(S579) and various neuronal markers (Figures 1H–1J). We used Car8, a Purkinje neuron marker in the cerebellum (Figure 1H); tyrosine hydroxylase (TH), a marker for dopaminergic neurons in the substantia nigra of the midbrain (Figure 1I); and NeuN, a marker for post-mitotic neurons, in the hippocampus (Figure 1J).

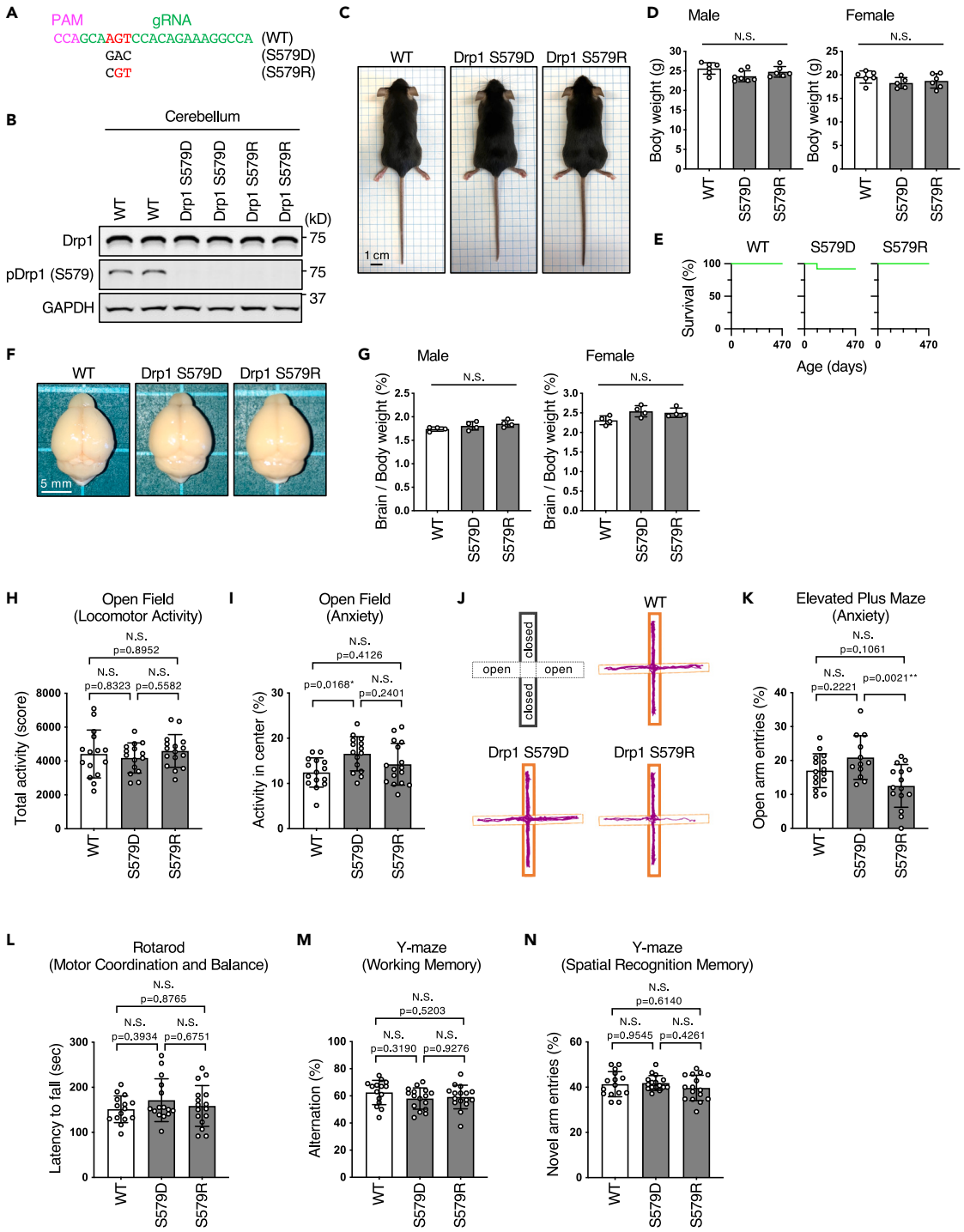

Figure 2. Behavior analysis of Drp1 S579D and S579R mice

(A) Drp1 S579D and S579R mice were generated using the CRISPR-Cas system. The gRNA target site is indicated in green. In the genetic modification, Drp1 S579 (AGT) was substituted with aspartic acid (D, GAC) and arginine (R, CGT).

(B) Western blot analysis of the cerebellum isolated from WT, Drp1 S579D, and Drp1 S579R mice was performed using the indicated antibodies.

(C) Representative images are shown of female WT, phospho-mimetic Drp1 S579D, and phospho-defective Drp1 S579R mice at 10 weeks of age.

(D) The body weight of 10-week-old mice is presented. Bars represent means ± SD (n = 5–7).

(E) Survival of mice is shown (n = 14 for WT mice, 13 for Drp1 S579D mice, and 16 for Drp1 S579R mice). Male and female mice are roughly equally represented.

(F) Representative images of brains dissected from female WT, Drp1 S579D, and Drp1 S579R mice at the age of 10 weeks are depicted.

Figure 2. *Continued*

(G) The relative ratios of brain weight to body weight in 10-week-old mice are shown. Bars represent means ± SD ($n = 4$). Statistical analysis was performed using one-way ANOVA in (D and G).

(H–N) Behavior tests were performed: (H and I) Open field test, where (H) locomotor activity was determined based on the total number of beam breaks in the central and peripheral regions, and (I) the percentages of beam breaks in the central region are presented. (J and K) Elevated plus maze test, with (J) representative track plots for each genotype, and (K) the percentages of entries into open arms.

(L) Rotarod test, measuring the latency to fall from the accelerating rotarod, with the average of three individual trials per mouse shown.

(M and N) Y-maze test, assessing the frequency of spontaneous alternation behavior (M) and entries into a novel arm (N). Bars represent means ± SD ($n = 12–16$ mice, with equal numbers of males and females analyzed). Statistical analysis was performed using one-way ANOVA with post hoc Tukey test in (H, I, K, L, M, and N), and p values are indicated.

In the cerebellum, a high level of pDrp1(S579) was co-localized with the Car8 signal, indicating that Drp1 S579 is highly phosphorylated in Purkinje neurons (Figure 1H). In the substantia nigra, a strong signal of pDrp1(S579) was observed in TH-positive dopaminergic neurons (Figure 1I). Similarly, in the hippocampus CA2 region, we noted colocalization of pDrp1(S579) with the NeuN signal (Figure 1J). To confirm the specificity of the pDrp1(S579) antibodies, we used a negative control: mice with a CRISPR-Cas-mediated mutation of the Drp1 gene (S579 changed to arginine, S579R). In these Drp1 S579R mice, pDrp1(S579) was not detected in the brain's frozen sections (Figures 1H–1J). These results collectively demonstrate that neurons, particularly in these regions of the brain, experience high levels of S579 phosphorylation. Further details on the generation of the phospho-defective Drp1 S579R mice and the phospho-mimetic S579D mice are provided in the following section.

Drp1 S579D and S579R mice have altered anxiety-related behaviors

To investigate the physiological role of S579 phosphorylated Drp1, we generated two mouse models: a Drp1 phospho-mimetic mutant (S579D) and a phospho-defective mutant (S579R), using the CRISPR-Cas system (Figures 2A and S1A). We used single-stranded DNA to introduce the S579D mutation, which changed the AGT codon (serine) to GAC (aspartic acid), resulting in the creation of phospho-mimetic Drp1 S579D mice (Figure 2A, S579D). Additionally, non-homologous end joining caused a single base pair change from A to C within the AGT codon. This alteration led to a substitution of serine (AGT) with arginine (CGT) in the phospho-defective Drp1 mice (Figure 2A, S579R). In Drp1 S579R mice, the loss of S579 phosphorylation in the brain was confirmed using western blotting (Figure 2B). Additionally, we observed that the anti-pDrp1(S579) antibodies did not recognize the Drp1 S579D protein in Drp1 S579D mice (Figure 2B). Physiological assessments revealed that both the Drp1 S579D and S579R mice maintained normal body weight (Figures 2C and 2D) and showed normal survival (Figure 2E). In addition, their brains developed to a size comparable to those of WT mice (Figures 2F and 2G). We also observed normal breeding in Drp1 S579D and S579R mice.

Given the high phosphorylation of S579 in brain neurons, we conducted five behavioral tests to assess how alterations in Drp1 S579 phosphorylation impact animal behaviors (Figures 2H–2N). In the open field test, both Drp1 S579D and S579R mice exhibited locomotor activities comparable to WT mice (Figure 2H). Notably, Drp1 S579D mice spent significantly more time in the central region than WT mice, suggesting a lower level of anxiety in the Drp1 S579D mice (Figure 2I). To further explore this observation, we conducted an elevated plus maze test to evaluate anxiety-like behaviors (Figures 2J and 2K). Consistent with the open field test results, Drp1 S579D mice spent more time in the open arm compared to WT mice, indicating potentially decreased anxiety, although this difference was modest and not statistically significant (Figures 2J and 2K). Interestingly, a comparison between Drp1 S579D and S579R mice showed that Drp1 S579R mice spent significantly less time in the open arm than Drp1 S579D mice (Figure 2K). In the rotarod test, both Drp1 S579D and S579R mice displayed normal motor coordination and balance (Figure 2L). Their performance in working memory (Figure 2M) and spatial recognition memory (Figure 2N) was also normal in Y-maze tests. These results suggest that Drp1 phosphorylation may play a role in regulating anxiety but does not appear to affect locomotion, coordination, or memory.

Mitochondrial morphology in neurons of Drp1 S579D and S579R mice

To investigate the impact of Drp1 S579D and S579R mutations on mitochondrial morphology, we utilized laser confocal immunofluorescence microscopy with antibodies to a mitochondrial matrix protein, Aco2, along with neuron-specific markers. These included Car8 for Purkinje neurons in the cerebellum (Figures 3A and 3B), TH for dopaminergic neurons in the substantia nigra (Figures 3C and 3D), and NeuN for neurons in the hippocampus (Figures 3E and 3F). Our observations revealed that the mitochondrial size was similar in WT, Drp1 S579D, and Drp1 S579R mice across neurons in all three examined regions. This indicates that phosphorylation at S579 does not significantly influence the overall mitochondrial size in these neuronal populations of mice under basal conditions.

S579 phosphorylation is increased during mitosis in the liver, heart, and skeletal muscle

It has been previously reported that Drp1 is phosphorylated at S579 during mitosis in *in vitro* culture systems.[38–41,43,44,54] To determine if S579 undergoes similar phosphorylation during mitosis *in vivo*, we analyzed S579 phosphorylation in mitotic cells of mouse tissues, including the liver, heart, and skeletal muscle. This analysis was performed using laser confocal immunofluorescence microscopy with antibodies to pDrp1(S579) and the mitotic marker phospho-histone H3 (pHistoneH3) (Figure 4A). For these experiments, we examined the livers of adult mice (aged 6–7 weeks) due to their relatively high mitotic capacity. In contrast, the heart and

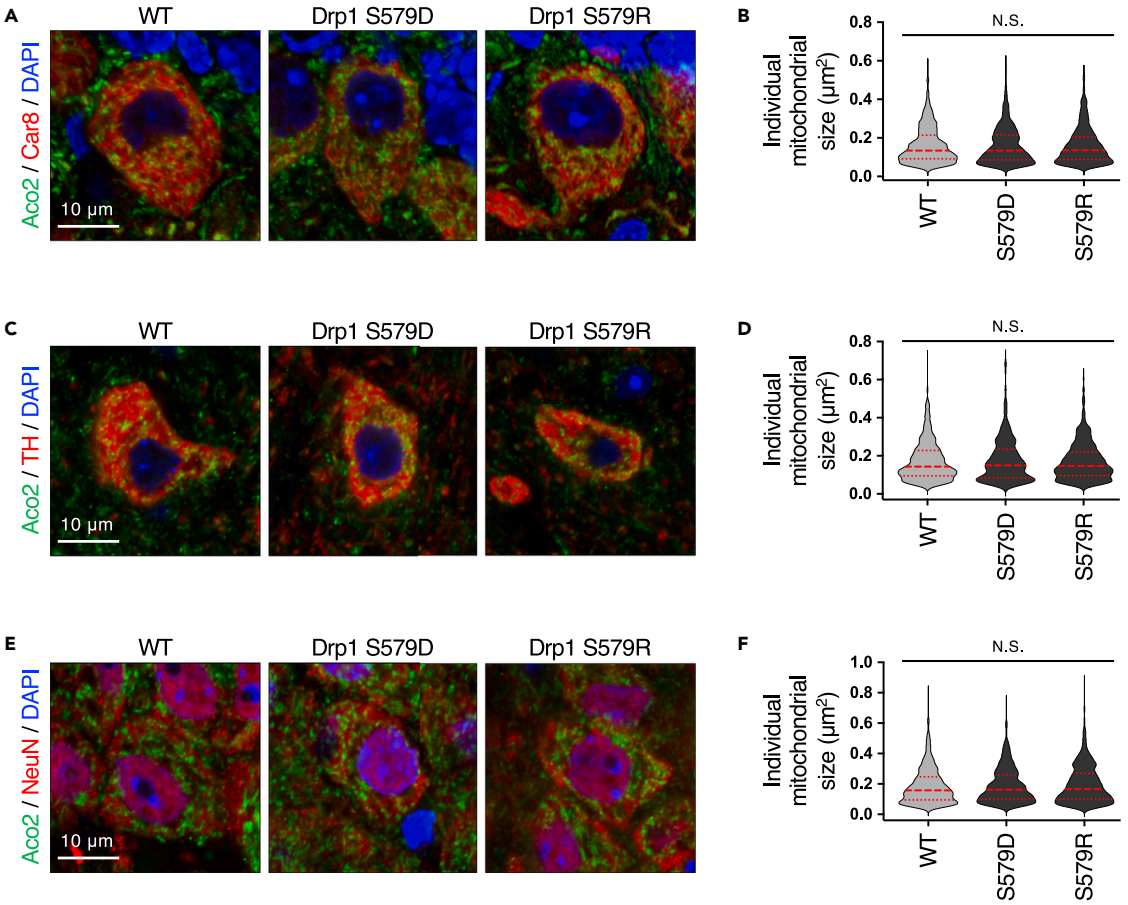

Figure 3. Mitochondrial morphology in neurons in WT, Drp1 S579D, and Drp1 S579R mice

(A–F) Immunofluorescence microscopy was performed on frozen brain sections of WT, Drp1 S579D, and Drp1 S579R mice. Antibodies against the mitochondrial protein Aco2 were used, alongside a Purkinje cell marker (Car8) in the cerebellum (A), a dopaminergic neuronal marker (TH) in the substantia nigra of the midbrain (C), and a post-mitotic neuron marker (NeuN) in the hippocampal CA2 region (E). (B, D, F) Quantification of mitochondrial size in Purkinje cells (n = 751–965 mitochondria from 3 mice) (B), dopaminergic neurons (n = 396–527 mitochondria from 3 mice) (D), and hippocampal neurons (n = 600–660 mitochondria from 3 mice) (F). Statistical analysis was performed using one-way ANOVA.

skeletal muscle were analyzed in younger mice (approximately 1.5 weeks old) as these tissues exhibit a lower frequency of mitosis compared to the liver in adult mice. We observed increased S579 phosphorylation in mitotic cells across the liver, heart, and skeletal muscle in WT mice (Figure 4A). Quantification confirmed significant increases in pDrp1(S579) signals in pHistoneH3-positive mitotic cells relative to pHistoneH3-negative interphase cells in the liver (Figure 4B). As a negative control, we utilized Drp1 S579R mouse and observed no S579 phosphorylation (Figures 4A and 4B). These findings suggest that Drp1 undergoes S579 phosphorylation during mitosis *in vivo*.

To determine if S579 phosphorylation is maintained throughout mitosis or is phase specific, we assessed S579 phosphorylation levels at prophase, metaphase, and telophase in WT MEFs. Laser confocal immunofluorescence microscopy was used, employing antibodies against pDrp1(S579) and pHistoneH3, along with DAPI staining. pHistoneH3 identified mitotic cells, while DAPI staining delineated the specific mitotic phase by chromosomal organization. Notably, anti-pDrp1(S579) antibodies revealed increased signals in both the cytoplasm and nucleus in mitotic cells (Figures 4A and 4B). In Drp1-KO MEFs, the cytoplasmic signal was absent, but the nuclear staining remained (Figures 4C and 4D), suggesting that nuclear staining does not reflect pDrp1(S579). The pDrp1(S579) signal was similarly elevated across all three phases (Figures 4C and 4D). Drp1 levels remained consistent in interphase and mitosis (Figures 4E and 4F), indicating that the increased pDrp1(S579) signal did not result from higher Drp1 expression.

Mitochondrial morphology in mitotic cells in Drp1 S579D and S579R mice

To assess whether the S579D and S579R mutations influence mitochondrial morphology in mitotic cells *in vivo*, we performed immunostaining on frozen liver sections from WT, Drp1 S579D, and S579R mice with antibodies targeting a mitochondrial matrix protein, Hsp60, and

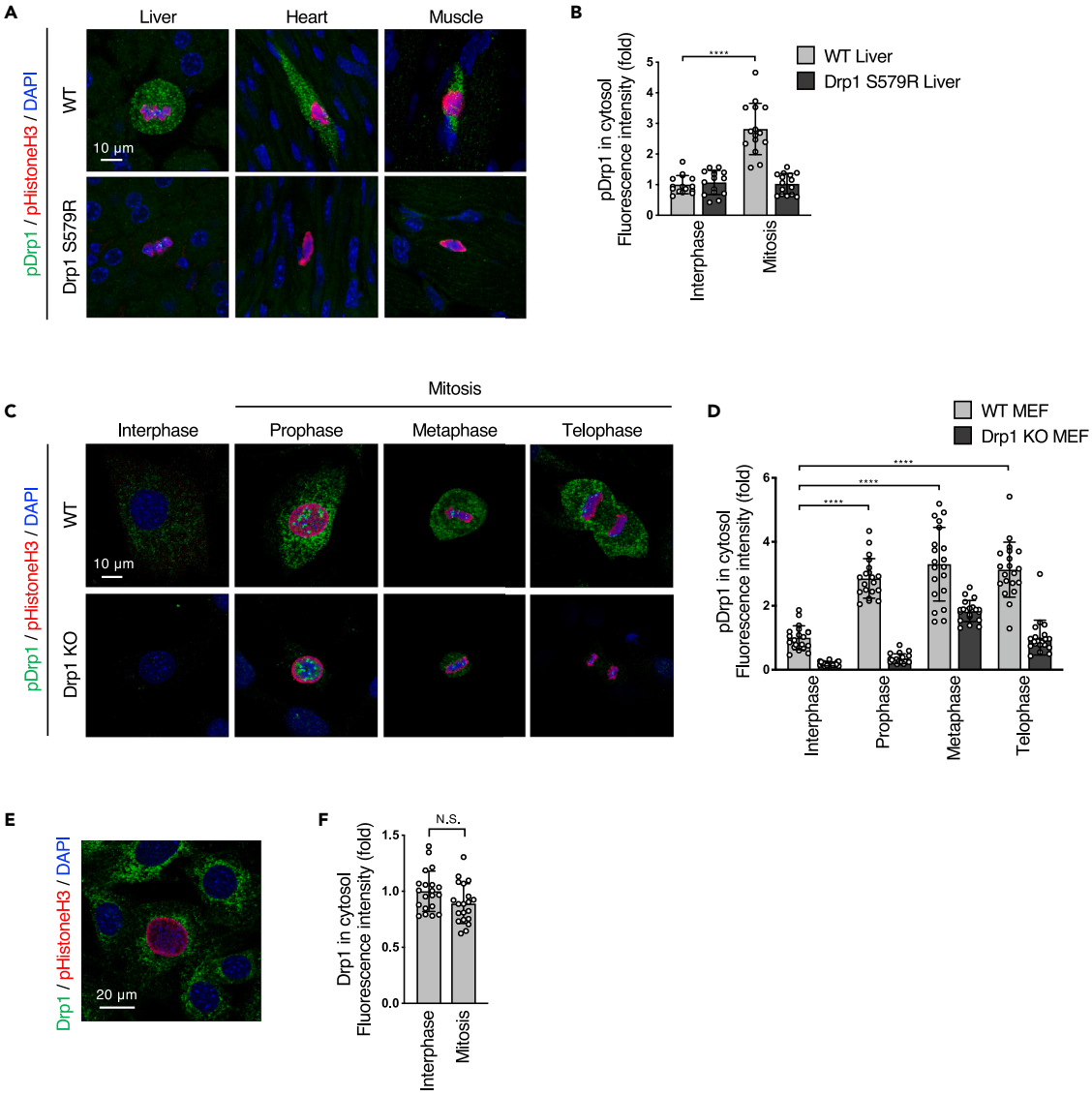

Figure 4. Drp1 S579 phosphorylation during mitosis *in vivo*

(A and B) Immunofluorescence analysis of Drp1 S579 phosphorylation *in vivo* was performed. (A) Frozen sections of the liver, heart, and skeletal muscle from WT and Drp1 S579R mice were immunostained with anti-pDrp1 S579 and -pHistoneH3 antibodies. (B) The intensity of pDrp1 S579 signal in the cytosol of pHistoneH3-negative interphase cells and pHistoneH3-positive mitotic cells in the liver was measured. Bars represent means ± SD (n = 3 mice, with 5 cells analyzed in each mouse).

(C and D) A comparison of Drp1 phosphorylation levels in MEFs during the interphase and mitotic phases was conducted. (C) Representative images of immunofluorescence staining with pDrp1 S579, pHistoneH3, and DAPI in WT and Drp1-KO MEFs are shown. (D) The intensity of pDrp1 S579 signal was quantified. Bars represent means ± SD (n = 20 cells).

(E and F) Drp1 levels in MEFs during the interphase and mitotic phases were compared. (E) A representative image shows immunofluorescence staining of Drp1 and pHistoneH3 in WT MEFs. (F) The intensity of Drp1 signal in the cytosol of interphase and mitotic cells was quantified in WT MEFs. Bars represent means ± SD (n = 20 cells). Statistical analysis was performed using one-way ANOVA with post hoc Tukey test in (B, D) and Student's t test in (F); ****$p < 0.0001$.

pHistoneH3. We found similar mitochondrial sizes in both interphase cells and pHistoneH3-positive mitotic cells across all three types of mice (Figures 5A and 5B). These observations suggest that mitochondrial morphology remains largely unchanged during mitosis in the liver. Additionally, despite the phosphorylation at S579, this modification does not seem to significantly affect mitochondrial morphology. Corroborating these *in vivo* results, mitochondria in Drp1-KO MEFs expressing WT Drp1, phospho-mimetic Drp1 (S579D), or phospho-defective Drp1 (S579A) also displayed similar sizes (Figure 5C). Moreover, the association of Drp1 with mitochondria appeared consistent regardless of the mutations (Figure 5C).

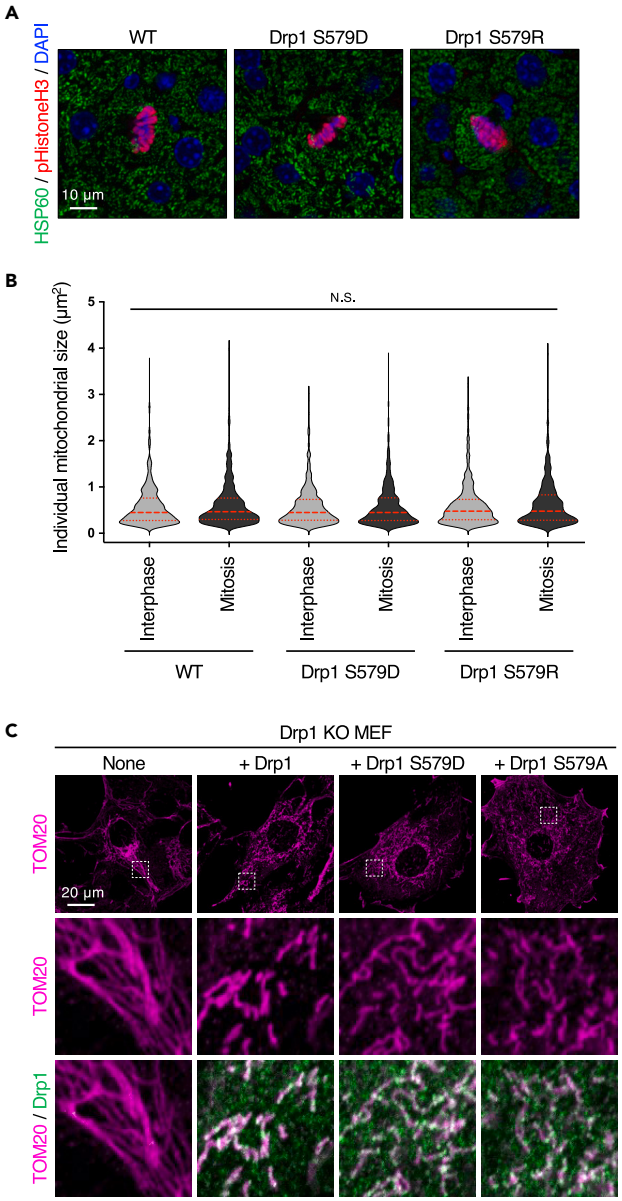

Figure 5. Mitochondrial morphology during mitosis *in vivo*

(A and B) Immunofluorescence analysis was performed to assess mitochondrial size in the liver of WT, Drp1 S579D, and Drp1 S579R mice during the interphase and mitotic phases. (A) Representative images show immunofluorescence staining of the mitochondrial marker Hsp60 and pHistoneH3. (B) The mitochondrial size was quantified in the interphase and mitotic cells in the liver. Dotted lines represent medians and quartiles (n = 403–533 mitochondria in 3 mice).

(C) Representative images illustrate immunofluorescence staining of the mitochondrial marker TOM20 and Drp1. Boxed areas in the images are enlarged. Elongated mitochondria in Drp1-KO MEFs became short tubules following the expression of WT Drp1, Drp1 S579D, and Drp1 S579A. Statistical analysis was performed using one-way ANOVA in (B).

DISCUSSION

Previous studies have extensively explored the mechanism and function of Drp1 S579 phosphorylation using cell culture systems and purified proteins.[33,38–41,43,44,54] In this current study, we have for the first time systematically analyzed Drp1 S579 phosphorylation in mouse tissues. We also examined the whole-body, physiological impact of this phosphorylation by generating Drp1 S579 phospho-mimetic (S579D) and phospho-defective (S579R) mice using the CRISPR-Cas genome-editing system.

We observed that Drp1 is highly phosphorylated at S579 in neurons throughout the brain. Given that neurons are primarily post-mitotic, these results imply that Drp1 S579 phosphorylation may have functions beyond mitosis. Indeed, we found that while the changes were

relatively modest, phospho-mimetic Drp1 S579D mice exhibited decreased anxiety-like behaviors, whereas phospho-defective Drp1 S579R mice displayed increased anxiety-like behaviors. Therefore, Drp1 phosphorylation at S579 may play a crucial role in neurons associated with anxiety control circuits, including the cortex, amygdala, hippocampus, and striatum.[55] A previous study reported that S-palmitoylation of Drp1 affects anxiety-like behaviors in mice.[56] Therefore, multiple post-translational modifications of Drp1 might be involved in regulating complex animal behaviors such as anxiety. Our findings also raise the possibility that pharmacological stimulation of Drp1 S579 phosphorylation could be a potential therapeutic strategy for treating anxiety-related disorders.

During embryonic development, neuronal stem cells are mitotic and actively proliferate to support brain growth.[57–59] The mitosis of neuronal stem cells is important for the proper regulation of cell fate determination in the developing brain.[58–60] At the same time, neuronal stem cells differentiate into specific types of neurons and glial cells in neurogenesis.[57–59] It is possible that the mitotic regulation of mitochondrial division is crucial in such neuronal stem cells for proper neurogenesis and thereby establishing neural circuits. In addition to mitotic regulation, mitochondrial division and fusion are important for cell fate determination in neurogenesis in post-mitotic neuronal stem cells.[59,61] We hypothesize that Drp1 phosphorylation regulates mitochondrial division during the mitosis of neural stem cells for brain development, and/or in post-mitotic neural stem cells for neurogenesis. We envision that a delicate balance between mitochondrial division and fusion plays critical roles in both processes, and alterations in these processes lead to altered animal behaviors, observed as changes in anxiety behaviors. It would be important and exciting to analyze the landscape of the neural population, their connectivity, and brain circuits in phospho-mimetic and phospho-defective Drp1 mice.

Previous research has demonstrated that Drp1 S579 phosphorylation intensifies under stress and in pathological conditions.[38–41,43,44,54] Our Drp1 S579D and S579R mice provide valuable *in vivo* models to explore the role of S579 phosphorylation in these scenarios. As mentioned in the Introduction, KRAS-driven transformation and tumorigenesis have been shown to rely on S579 phosphorylation of Drp1.[40,41] Additionally, Drp1 S579 phosphorylation has been linked to cell death induced by NMDA in cultured neurons.[44] Investigating these processes with the Drp1 S579D and S579R mice could significantly deepen our understanding of these pathological mechanisms at the animal level and potentially aid in developing Drp1 phosphorylation-targeted therapeutic strategies.

Contrary to Drp1-KO mice, which exhibit embryonic lethality,[46] Drp1 S579D and S579R mice appeared to grow, develop, and breed normally. This outcome was surprising, given that Drp1 S579 phosphorylation is known to regulate mitochondrial size during mitosis. Additionally, we observed that the mitochondrial morphology in mitotic cells of the liver, heart, and skeletal muscle in these mice remained consistent. This suggests that the requirement for mitochondrial fragmentation during mitosis might be cell type specific, and the cells in our study may undergo mitosis without activating mitochondrial division. This idea aligns with findings that Drp1-KO MEFs continue to grow and distribute mitochondria into daughter cells normally.[13,48,62] Similarly, it has been shown that even without mitochondrial division in hepatocytes, the liver in Drp1-KO mice can attain a normal size, though some tissue damage was observed.[50] Alternatively, the absence of S579 phosphorylation might be counterbalanced by other regulatory mechanisms during development, as Drp1 is also subject to additional phosphorylation at S600, as well as other post-translational modifications like ubiquitination, SUMOylation, and O-GlcNAcylation.[16] Investigating the effects of Drp1 S579D and S579R mutations acutely in adult mice would be an intriguing and important future study, as it could bypass potential compensatory mechanisms that may occur during embryonic development.

Finally, mutations in Drp1 and its receptor Mff lead to human conditions characterized by neurodevelopmental defects, microcephaly, refractory epilepsy, hypotonia, ataxia, seizures, and optic atrophy.[63–68] Therefore, it is crucial to decipher the regulation of Drp1-mediated mitochondrial division and translate this fundamental knowledge into therapeutic interventions to treat mitochondrial division-associated diseases and improve human health.

Limitations of the study

In the present study, our investigation was limited to examining Drp1 S579D and S579R mice under physiological conditions, where we found no significant changes in mitochondrial morphology and animal survival. Since Drp1 activity undergoes various regulations and alterations in response to mitochondrial stress and pathological conditions, it would be of great interest to examine how Drp1 phosphorylation changes and how these mice respond to different stressors and disease inducers in future studies. Such investigations potentially underscore the pathophysiological role of Drp1 regulation *in vivo*.

STAR★METHODS

Detailed methods are provided in the online version of this paper and include the following:

- KEY RESOURCES TABLE
- RESOURCE AVAILABILITY
  - Lead contact
  - Materials availability
  - Data and code availability
- EXPERIMENTAL MODEL AND STUDY PARTICIPANT DETAILS
  - Animals
  - Cells
- METHOD DETAILS

- Lentiviruses
- Western blotting
- Immunofluorescence microscopy on mouse tissue sections
- Immunofluorescence microscopy on MEFs
- Behavior analysis

- QUANTIFICATION AND STATISTICAL ANALYSIS

SUPPLEMENTAL INFORMATION

Supplemental information can be found online at https://doi.org/10.1016/j.isci.2024.109874.

ACKNOWLEDGMENTS

We thank members of the Iijima and Sesaki labs for invaluable discussions and technical assistance. This work was supported by NIH grants to M.I. (GM131768) and H.S. (GM144103) and by Uehara Foundation Postdoctoral Fellowship to A.I.

AUTHOR CONTRIBUTIONS

A.I., M.I., and H.S. designed the study, performed the experiments, analyzed the data, and wrote the manuscript.

DECLARATION OF INTERESTS

The authors declare no competing financial interests.

Received: January 31, 2024
Revised: April 21, 2024
Accepted: April 29, 2024
Published: May 3, 2024

REFERENCES

1. Murata, D., Arai, K., Iijima, M., and Sesaki, H. (2020). Mitochondrial division, fusion and degradation. J. Biochem. *167*, 233–241. https://doi.org/10.1093/jb/mvz106.
2. Kameoka, S., Adachi, Y., Okamoto, K., Iijima, M., and Sesaki, H. (2018). Phosphatidic Acid and Cardiolipin Coordinate Mitochondrial Dynamics. Trends Cell Biol. *28*, 67–76. https://doi.org/10.1016/j.tcb.2017.08.011.
3. Quintana-Cabrera, R., and Scorrano, L. (2023). Determinants and outcomes of mitochondrial dynamics. Mol. Cell *83*, 857–876. https://doi.org/10.1016/j.molcel.2023.02.012.
4. Roy, M., Reddy, P.H., Iijima, M., and Sesaki, H. (2015). Mitochondrial division and fusion in metabolism. Curr. Opin. Cell Biol. *33*, 111–118. https://doi.org/10.1016/j.ceb.2015.02.001.
5. Itoh, K., Nakamura, K., Iijima, M., and Sesaki, H. (2013). Mitochondrial dynamics in neurodegeneration. Trends Cell Biol. *23*, 64–71. https://doi.org/10.1016/j.tcb.2012.10.006.
6. Liesa, M., and Shirihai, O.S. (2013). Mitochondrial dynamics in the regulation of nutrient utilization and energy expenditure. Cell Metab. *17*, 491–506. https://doi.org/10.1016/j.cmet.2013.03.002.
7. Serasinghe, M.N., and Chipuk, J.E. (2017). Mitochondrial Fission in Human Diseases. Handb. Exp. Pharmacol. *240*, 159–188. https://doi.org/10.1007/164_2016_38.
8. Mishra, P., and Chan, D.C. (2014). Mitochondrial dynamics and inheritance during cell division, development and disease. Nat. Rev. Mol. Cell Biol. *15*, 634–646. https://doi.org/10.1038/nrm3877.
9. Kashatus, D.F. (2018). The regulation of tumor cell physiology by mitochondrial dynamics. Biochem. Biophys. Res. Commun. *500*, 9–16. https://doi.org/10.1016/j.bbrc.2017.06.192.
10. Kraus, F., Roy, K., Pucadyil, T.J., and Ryan, M.T. (2021). Function and regulation of the divisome for mitochondrial fission. Nature *590*, 57–66. https://doi.org/10.1038/s41586-021-03214-x.
11. Fung, T.S., Chakrabarti, R., and Higgs, H.N. (2023). The multiple links between actin and mitochondria. Nat. Rev. Mol. Cell Biol. *24*, 651–667. https://doi.org/10.1038/s41580-023-00613-y.
12. Tamura, Y., Itoh, K., and Sesaki, H. (2011). SnapShot: Mitochondrial dynamics. Cell *145*, 1158–1158.e1. https://doi.org/10.1016/j.cell.2011.06.018.
13. Adachi, Y., Itoh, K., Yamada, T., Cerveny, K.L., Suzuki, T.L., Macdonald, P., Frohman, M.A., Ramachandran, R., Iijima, M., and Sesaki, H. (2016). Coincident Phosphatidic Acid Interaction Restrains Drp1 in Mitochondrial Division. Mol. Cell *63*, 1034–1043. https://doi.org/10.1016/j.molcel.2016.08.013.
14. Itoh, K., Adachi, Y., Yamada, T., Suzuki, T.L., Otomo, T., McBride, H.M., Yoshimori, T., Iijima, M., and Sesaki, H. (2018). A brain-enriched Drp1 isoform associates with lysosomes, late endosomes, and the plasma membrane. J. Biol. Chem. *293*, 11809–11822. https://doi.org/10.1074/jbc.RA117.001253.
15. Itoh, K., Murata, D., Kato, T., Yamada, T., Araki, Y., Saito, A., Adachi, Y., Igarashi, A., Li, S., Pletnikov, M., et al. (2019). Brain-specific Drp1 regulates postsynaptic endocytosis and dendrite formation independently of mitochondrial division. Elife *8*, e44739. https://doi.org/10.7554/eLife.44739.
16. Munoz, J.P., Basei, F.L., Rojas, M.L., Galvis, D., and Zorzano, A. (2023). Mechanisms of Modulation of Mitochondrial Architecture. Biomolecules *13*, 1225. https://doi.org/10.3390/biom13081225.
17. Nichols, J.M.E., Paschke, P., Peak-Chew, S., Williams, T.D., Tweedy, L., Skehel, M., Stephens, E., Chubb, J.R., and Kay, R.R. (2019). The Atypical MAP Kinase ErkB Transmits Distinct Chemotactic Signals through a Core Signaling Module. Dev. Cell *48*, 491–505.e9. https://doi.org/10.1016/j.devcel.2018.12.001.
18. Yu, T., Jhun, B.S., and Yoon, Y. (2011). High-glucose stimulation increases reactive oxygen species production through the calcium and mitogen-activated protein kinase-mediated activation of mitochondrial fission. Antioxid. Redox Signal. *14*, 425–437. https://doi.org/10.1089/ars.2010.3284.
19. Qi, X., Disatnik, M.H., Shen, N., Sobel, R.A., and Mochly-Rosen, D. (2011). Aberrant mitochondrial fission in neurons induced by protein kinase Cdelta under oxidative stress conditions *in vivo*. Mol. Biol. Cell *22*, 256–265. https://doi.org/10.1091/mbc.E10-06-0551.
20. Qu, C., Yang, W., Kan, Y., Zuo, H., Wu, M., Zhang, Q., Wang, H., Wang, D., and Chen, J. (2022). RhoA/ROCK Signaling Regulates Drp1-Mediated Mitochondrial Fission During Collective Cell Migration. Front. Cell Dev. Biol. *10*, 882581. https://doi.org/10.3389/fcell.2022.882581.
21. Xu, S., Wang, P., Zhang, H., Gong, G., Gutierrez Cortes, N., Zhu, W., Yoon, Y., Tian, R., and Wang, W. (2016). CaMKII induces permeability transition through Drp1 phosphorylation during chronic beta-AR stimulation. Nat. Commun. *7*, 13189. https://doi.org/10.1038/ncomms13189.
22. Han, H., Tan, J., Wang, R., Wan, H., He, Y., Yan, X., Guo, J., Gao, Q., Li, J., Shang, S., et al. (2020). PINK1 phosphorylates Drp1(S616) to

regulate mitophagy-independent mitochondrial dynamics. EMBO Rep. *21*, e48686. https://doi.org/10.15252/embr.201948686.

23. Chang, C.R., and Blackstone, C. (2007). Cyclic AMP-dependent protein kinase phosphorylation of Drp1 regulates its GTPase activity and mitochondrial morphology. J. Biol. Chem. *282*, 21583–21587.
24. Cribbs, J.T., and Strack, S. (2007). Reversible phosphorylation of Drp1 by cyclic AMP-dependent protein kinase and calcineurin regulates mitochondrial fission and cell death. EMBO Rep. *8*, 939–944. https://doi.org/10.1038/sj.embor.7401062.
25. Wang, W., Wang, Y., Long, J., Wang, J., Haudek, S.B., Overbeek, P., Chang, B.H.J., Schumacker, P.T., and Danesh, F.R. (2012). Mitochondrial fission triggered by hyperglycemia is mediated by ROCK1 activation in podocytes and endothelial cells. Cell Metab. *15*, 186–200. https://doi.org/10.1016/j.cmet.2012.01.009.
26. Han, X.J., Lu, Y.F., Li, S.A., Kaitsuka, T., Sato, Y., Tomizawa, K., Nairn, A.C., Takei, K., Matsui, H., and Matsushita, M. (2008). CaM kinase I alpha-induced phosphorylation of Drp1 regulates mitochondrial morphology. J. Cell Biol. *182*, 573–585.
27. Wikstrom, J.D., Israeli, T., Bachar-Wikstrom, E., Swisa, A., Ariav, Y., Waiss, M., Kaganovich, D., Dor, Y., Cerasi, E., and Leibowitz, G. (2013). AMPK regulates ER morphology and function in stressed pancreatic beta-cells via phosphorylation of DRP1. Mol. Endocrinol. *27*, 1706–1723. https://doi.org/10.1210/me.2013-1109.
28. Jhun, B.S., O-Uchi, J., Adaniya, S.M., Mancini, T.J., Cao, J.L., King, M.E., Landi, A.K., Ma, H., Shin, M., Yang, D., et al. (2018). Protein kinase D activation induces mitochondrial fragmentation and dysfunction in cardiomyocytes. J. Physiol. *596*, 827–855. https://doi.org/10.1113/JP275418.
29. Cereghetti, G.M., Stangherlin, A., Martins de Brito, O., Chang, C.R., Blackstone, C., Bernardi, P., and Scorrano, L. (2008). Dephosphorylation by calcineurin regulates translocation of Drp1 to mitochondria. Proc. Natl. Acad. Sci. USA *105*, 15803–15808.
30. Galvan, D.L., Long, J., Green, N., Chang, B.H., Lin, J.S., Schumacker, P., Truong, L.D., Overbeek, P., and Danesh, F.R. (2019). Drp1S600 phosphorylation regulates mitochondrial fission and progression of nephropathy in diabetic mice. J. Clin. Invest. *129*, 2807–2823. https://doi.org/10.1172/JCI127277.
31. Yu, R., Liu, T., Ning, C., Tan, F., Jin, S.B., Lendahl, U., Zhao, J., and Nistér, M. (2019). The phosphorylation status of Ser-637 in dynamin-related protein 1 (Drp1) does not determine Drp1 recruitment to mitochondria. J. Biol. Chem. *294*, 17262–17277. https://doi.org/10.1074/jbc.RA119.008202.
32. Valera-Alberni, M., Joffraud, M., Miro-Blanch, J., Capellades, J., Junza, A., Dayon, L., Núñez Galindo, A., Sanchez-Garcia, J.L., Valsesia, A., Cercillieux, A., et al. (2021). Crosstalk between Drp1 phosphorylation sites during mitochondrial remodeling and their impact on metabolic adaptation. Cell Rep. *36*, 109565. https://doi.org/10.1016/j.celrep.2021.109565.
33. Liu, A., Hatch, A.L., and Higgs, H.N. (2024). Effects of phosphorylation on Drp1 activation by its receptors, actin, and cardiolipin. Mol. Biol. Cell *35*, ar16. https://doi.org/10.1091/mbc.E23-11-0427.
34. Strack, S., Wilson, T.J., and Cribbs, J.T. (2013). Cyclin-dependent kinases regulate splice-specific targeting of dynamin-related protein 1 to microtubules. J. Cell Biol. *201*, 1037–1051. https://doi.org/10.1083/jcb.201210045.
35. Boissan, M., Montagnac, G., Shen, Q., Griparic, L., Guitton, J., Romao, M., Sauvonnet, N., Lagache, T., Lascu, I., Raposo, G., et al. (2014). Membrane trafficking. Nucleoside diphosphate kinases fuel dynamin superfamily proteins with GTP for membrane remodeling. Science *344*, 1510–1515. https://doi.org/10.1126/science.1253768.
36. Abe, Y., Wanders, R.J.A., Waterham, H.R., Mandel, H., Falik-Zaccai, T.C., Ishihara, N., and Fujiki, Y. (2023). Genetic defects in peroxisome morphogenesis (Pex11beta, dynamin-like protein 1, and nucleoside diphosphate kinase 3) affect docosahexaenoic acid-phospholipid metabolism. J. Inherit. Metab. Dis. *46*, 273–285. https://doi.org/10.1002/jimd.12582.
37. Su, Y.A., Chiu, H.Y., Chang, Y.C., Sung, C.J., Chen, C.W., Tei, R., Huang, X.R., Hsu, S.C., Lin, S.S., Wang, H.C., et al. (2023). NME3 binds to phosphatidic acid and mediates PLD6-induced mitochondrial tethering. J. Cell Biol. *222*, e202301091. https://doi.org/10.1083/jcb.202301091.
38. Taguchi, N., Ishihara, N., Jofuku, A., Oka, T., and Mihara, K. (2007). Mitotic phosphorylation of dynamin-related GTPase Drp1 participates in mitochondrial fission. J. Biol. Chem. *282*, 11521–11529. https://doi.org/10.1074/jbc.M607279200.
39. Kashatus, D.F., Lim, K.H., Brady, D.C., Pershing, N.L.K., Cox, A.D., and Counter, C.M. (2011). RALA and RALBP1 regulate mitochondrial fission at mitosis. Nat. Cell Biol. *13*, 1108–1115. https://doi.org/10.1038/ncb2310.
40. Kashatus, J.A., Nascimento, A., Myers, L.J., Sher, A., Byrne, F.L., Hoehn, K.L., Counter, C.M., and Kashatus, D.F. (2015). Erk2 phosphorylation of Drp1 promotes mitochondrial fission and MAPK-driven tumor growth. Mol. Cell *57*, 537–551. https://doi.org/10.1016/j.molcel.2015.01.002.
41. Serasinghe, M.N., Wieder, S.Y., Renault, T.T., Elkholi, R., Asciolla, J.J., Yao, J.L., Jabado, O., Hoehn, K., Kageyama, Y., Sesaki, H., and Chipuk, J.E. (2015). Mitochondrial Division Is Requisite to RAS-Induced Transformation and Targeted by Oncogenic MAPK Pathway Inhibitors. Mol. Cell *57*, 521–536. https://doi.org/10.1016/j.molcel.2015.01.003.
42. Prieto, J., León, M., Ponsoda, X., Sendra, R., Bort, R., Ferrer-Lorente, R., Raya, A., López-García, C., and Torres, J. (2016). Early ERK1/2 activation promotes DRP1-dependent mitochondrial fission necessary for cell reprogramming. Nat. Commun. *7*, 11124. https://doi.org/10.1038/ncomms11124.
43. Yuan, Y., Chen, J., Ge, X., Deng, J., Xu, X., Zhao, Y., and Wang, H. (2021). Activation of ERK-Drp1 signaling promotes hypoxia-induced Abeta accumulation by upregulating mitochondrial fission and BACE1 activity. FEBS Open Bio *11*, 2740–2755. https://doi.org/10.1002/2211-5463.13273.
44. Jahani-Asl, A., Huang, E., Irrcher, I., Rashidian, J., Ishihara, N., Lagace, D.C., Slack, R.S., and Park, D.S. (2015). CDK5 phosphorylates DRP1 and drives mitochondrial defects in NMDA-induced neuronal death. Hum. Mol. Genet. *24*, 4573–4583. https://doi.org/10.1093/hmg/ddv188.
45. Park, H.S., Liu, G., Liu, Q., and Zhou, Y. (2018). Swine Influenza Virus Induces RIPK1/DRP1-Mediated Interleukin-1 Beta Production. Viruses *10*, 419. https://doi.org/10.3390/v10080419.
46. Wakabayashi, J., Zhang, Z., Wakabayashi, N., Tamura, Y., Fukaya, M., Kensler, T.W., Iijima, M., and Sesaki, H. (2009). The dynamin-related GTPase Drp1 is required for embryonic and brain development in mice. J. Cell Biol. *186*, 805–816.
47. Ishihara, N., Nomura, M., Jofuku, A., Kato, H., Suzuki, S.O., Masuda, K., Otera, H., Nakanishi, Y., Nonaka, I., Goto, Y.I., et al. (2009). Mitochondrial fission factor Drp1 is essential for embryonic development and synapse formation in mice. Nat. Cell Biol. *11*, 958–966. https://doi.org/10.1038/ncb1907.
48. Kageyama, Y., Hoshijima, M., Seo, K., Bedja, D., Sysa-Shah, P., Andrabi, S.A., Chen, W., Höke, A., Dawson, V.L., Dawson, T.M., et al. (2014). Parkin-independent mitophagy requires Drp1 and maintains the integrity of mammalian heart and brain. EMBO J. *33*, 2798–2813. https://doi.org/10.15252/embj.201488658.
49. Song, M., Mihara, K., Chen, Y., Scorrano, L., and Dorn, G.W., 2nd (2015). Mitochondrial fission and fusion factors reciprocally orchestrate mitophagic culling in mouse hearts and cultured fibroblasts. Cell Metab. *21*, 273–286. https://doi.org/10.1016/j.cmet.2014.12.011.
50. Yamada, T., Murata, D., Adachi, Y., Itoh, K., Kameoka, S., Igarashi, A., Kato, T., Araki, Y., Huganir, R.L., Dawson, T.M., et al. (2018). Mitochondrial Stasis Reveals p62-Mediated Ubiquitination in Parkin-Independent Mitophagy and Mitigates Nonalcoholic Fatty Liver Disease. Cell Metab. *28*, 588–604.e5. https://doi.org/10.1016/j.cmet.2018.06.014.
51. Kageyama, Y., Zhang, Z., Roda, R., Fukaya, M., Wakabayashi, J., Wakabayashi, N., Kensler, T.W., Reddy, P.H., Iijima, M., and Sesaki, H. (2012). Mitochondrial division ensures the survival of postmitotic neurons by suppressing oxidative damage. J. Cell Biol. *197*, 535–551. https://doi.org/10.1083/jcb.201110034.
52. Berthet, A., Margolis, E.B., Zhang, J., Hsieh, I., Zhang, J., Hnasko, T.S., Ahmad, J., Edwards, R.H., Sesaki, H., Huang, E.J., and Nakamura, K. (2014). Loss of mitochondrial fission depletes axonal mitochondria in midbrain dopamine neurons. J. Neurosci. *34*, 14304–14317. https://doi.org/10.1523/JNEUROSCI.0930-14.2014.
53. Shields, L.Y., Kim, H., Zhu, L., Haddad, D., Berthet, A., Pathak, D., Lam, M., Ponnusamy, R., Diaz-Ramirez, L.G., Gill, T.M., et al. (2015). Dynamin-related protein 1 is required for normal mitochondrial bioenergetic and synaptic function in CA1 hippocampal neurons. Cell Death Dis. *6*, e1725. https://doi.org/10.1038/cddis.2015.94.
54. Guo, M.Y., Shang, L., Hu, Y.Y., Jiang, L.P., Wan, Y.Y., Zhou, Q.Q., Zhang, K., Liao, H.F., Yi, J.L., and Han, X.J. (2018). The role of Cdk5-mediated Drp1 phosphorylation in Abeta(1-42) induced mitochondrial fission and neuronal apoptosis. J. Cell. Biochem. *119*, 4815–4825. https://doi.org/10.1002/jcb.26680.
55. Hollis, F., van der Kooij, M.A., Zanoletti, O., Lozano, L., Cantó, C., and Sandi, C. (2015). Mitochondrial function in the brain links anxiety with social subordination. Proc. Natl. Acad. Sci. USA *112*, 15486–15491. https://doi.org/10.1073/pnas.1512653112.

56. Napoli, E., Song, G., Liu, S., Espejo, A., Perez, C.J., Benavides, F., and Giulivi, C. (2017). Zdhhc13-dependent Drp1 S-palmitoylation impacts brain bioenergetics, anxiety, coordination and motor skills. Sci. Rep. *7*, 12796. https://doi.org/10.1038/s41598-017-12889-0.

57. Ozgen, S., Krigman, J., Zhang, R., and Sun, N. (2022). Significance of mitochondrial activity in neurogenesis and neurodegenerative diseases. Neural Regen. Res. *17*, 741–747. https://doi.org/10.4103/1673-5374.322429.

58. Petridi, S., Dubal, D., Rikhy, R., and van den Ameele, J. (2022). Mitochondrial respiration and dynamics of *in vivo* neural stem cells. Development *149*, dev200870. https://doi.org/10.1242/dev.200870.

59. Scandella, V., Petrelli, F., Moore, D.L., Braun, S.M.G., and Knobloch, M. (2023). Neural stem cell metabolism revisited: a critical role for mitochondria. Trends Endocrinol. Metab. *34*, 446–461. https://doi.org/10.1016/j.tem.2023.05.008.

60. Pilaz, L.J., McMahon, J.J., Miller, E.E., Lennox, A.L., Suzuki, A., Salmon, E., and Silver, D.L. (2016). Prolonged Mitosis of Neural Progenitors Alters Cell Fate in the Developing Brain. Neuron *89*, 83–99. https://doi.org/10.1016/j.neuron.2015.12.007.

61. Iwata, R., Casimir, P., and Vanderhaeghen, P. (2020). Mitochondrial dynamics in postmitotic cells regulate neurogenesis. Science *369*, 858–862. https://doi.org/10.1126/science.aba9760.

62. Murata, D., Yamada, T., Tokuyama, T., Arai, K., Quirós, P.M., López-Otín, C., Iijima, M., and Sesaki, H. (2020). Mitochondrial Safeguard: a stress response that offsets extreme fusion and protects respiratory function via flickering-induced Oma1 activation. EMBO J. *39*, e105074. https://doi.org/10.15252/embj.2020105074.

63. Whitley, B.N., Lam, C., Cui, H., Haude, K., Bai, R., Escobar, L., Hamilton, A., Brady, L., Tarnopolsky, M.A., Dengle, L., et al. (2018). Aberrant Drp1-mediated mitochondrial division presents in humans with variable outcomes. Hum. Mol. Genet. *27*, 3710–3719. https://doi.org/10.1093/hmg/ddy287.

64. Fahrner, J.A., Liu, R., Perry, M.S., Klein, J., and Chan, D.C. (2016). A novel *de novo* dominant negative mutation in DNM1L impairs mitochondrial fission and presents as childhood epileptic encephalopathy. Am. J. Med. Genet. *170*, 2002–2011. https://doi.org/10.1002/ajmg.a.37721.

65. Verrigni, D., Di Nottia, M., Ardissone, A., Baruffini, E., Nasca, A., Legati, A., Bellacchio, E., Fagiolari, G., Martinelli, D., Fusco, L., et al. (2019). Clinical-genetic features and peculiar muscle histopathology in infantile DNM1L-related mitochondrial epileptic encephalopathy. Hum. Mutat. *40*, 601–618. https://doi.org/10.1002/humu.23729.

66. Murata, D., Grunseich, C., Iijima, M., Chan, D., Corse, A., Hoke, A., Schindler, A., Sesaki, H., and Roda, R.H. (2023). A Heterozygous Mutation in MFF Associated with a Mild Mitochondrial Phenotype. J. Neuromuscul. Dis. *10*, 107–118. https://doi.org/10.3233/JND-221532.

67. Sharma, C., Saini, A., Gothwal, M., Jhirwal, M., and Patwa, P. (2021). Mitochondrial Fission Factor Gene Mutation: A Dilemma for Prenatal Diagnosis. Int. J. Appl. Basic Med. Res. *11*, 114–116. https://doi.org/10.4103/ijabmr.IJABMR_355_20.

68. Panda, I., Ahmad, I., Sagar, S., Zahra, S., Shamim, U., Sharma, S., and Faruq, M. (2020). Encephalopathy due to defective mitochondrial and peroxisomal fission 2 caused by a novel MFF gene mutation in a young child. Clin. Genet. *97*, 933–937. https://doi.org/10.1111/cge.13740.

69. Stewart, S.A., Dykxhoorn, D.M., Palliser, D., Mizuno, H., Yu, E.Y., An, D.S., Sabatini, D.M., Chen, I.S.Y., Hahn, W.C., Sharp, P.A., et al. (2003). Lentivirus-delivered stable gene silencing by RNAi in primary cells. RNA *9*, 493–501.

70. Yamada, T., Dawson, T.M., Yanagawa, T., Iijima, M., and Sesaki, H. (2019). SQSTM1/p62 promotes mitochondrial ubiquitination independently of PINK1 and PRKN/parkin in mitophagy. Autophagy *15*, 2012–2018. https://doi.org/10.1080/15548627.2019.1643185.

71. Adachi, Y., Kato, T., Yamada, T., Murata, D., Arai, K., Stahelin, R.V., Chan, D.C., Iijima, M., and Sesaki, H. (2020). Drp1 Tubulates the ER in a GTPase-Independent Manner. Mol. Cell *80*, 621–632.e6. https://doi.org/10.1016/j.molcel.2020.10.013.

STAR★METHODS

KEY RESOURCES TABLE

REAGENT or RESOURCE	SOURCE	IDENTIFIER
Antibodies		
Mouse monoclonal anti-Drp1	BD Biosciences	Cat#611113; RRID: AB_398424
Rabbit polyclonal anti-phospho-Drp1 (human Ser616/mouse S579)	Cell Signaling Technology	Cat#3455; RRID: AB_2085352
Mouse monoclonal anti-Pyruvate dehydrogenase E2/E3bp	Abcam	Cat#ab110333; RRID: AB_10862029
Mouse monoclonal anti-GAPDH	Thermo Fisher Scientific	Cat#MA5-15738; RRID: AB_10977387
Goat polyclonal anti-Car8	Frontier Institute	Cat#Car8-Go-Af780; RRID: AB_2571668
Goat polyclonal anti-Tyrosine Hydroxylase	Abcam	Cat#ab101853; RRID: AB_10710873
Mouse monoclonal anti-NeuN	Sigma-Aldrich	Cat#MAB377; RRID: AB_2298772
Mouse monoclonal anti-phospho-Histone H3 (Ser10)	Invitrogen	Cat#MA6-15220; RRID: AB_11008586
Rabbit monoclonal anti-HSP60	Cell Signaling Technology	Cat#12165; RRID: AB_2636980
Rabbit polyclonal anti-Aconitase 2	Proteintech	Cat#11134-1-AP; RRID: AB_2289288
Mouse monoclonal anti-Drp1	Cell Signaling Technology	Cat#8570; RRID: AB_10950498
Rabbit polyclonal anti-TOM20	Proteintech	Cat#11802-1-AP; RRID: AB_2207530
Alexa 488 anti-rabbit IgG	Invitrogen	Cat#A21206; RRID: AB_2535792
Alexa 488 anti-mouse IgG	Invitrogen	Cat#A21202; RRID: AB_141607
Alexa 568 anti-rabbit IgG	Invitrogen	Cat#A10042; RRID: AB_2534017
Alexa 568 anti-mouse IgG	Invitrogen	Cat#A10037; RRID: AB_2534013
Alexa 568 anti-goat IgG	Invitrogen	Cat#A11057; RRID: AB_2534104
Chemicals, peptides, and recombinant proteins		
2-Methyl-2-butanol	Sigma-Aldrich	Cat#240486
2,2,2-Tribromoethanol	Sigma-Aldrich	Cat#T48402
Paraformaldehyde	Sigma-Aldrich	Cat#P6148
PBS (10X)	Quality Biological	Cat#119-069-131
cOmplete, Mini, EDTA-free Protease Inhibitor Cocktail	Roche	Cat#11836170001
Phosphatase Inhibitor Cocktail 2	Sigma-Aldrich	Cat#P5726
Phosphatase Inhibitor Cocktail 3	Sigma-Aldrich	Cat#P0044
Bio-Rad Protein Assay Dye Reagent Concentrate	Bio-Rad	Cat#5000006
Immobilon-FL PVDF Membrane	Millipore	Cat#IPFL00010
IMDM	Gibco	Cat#12440053
Dulbecco's Modified Eagle's Medium – high glucose	Sigma-Aldrich	Cat#D5796
Dulbecco's Phosphate Buffered Saline	Sigma-Aldrich	Cat#D8537
Fetal Bovine Serum	Sigma-Aldrich	Cat#F6178
Lipofectamine 3000 Transfection Reagent	Invitrogen	Cat#L3000001
Tissue-Tek O.C.T. Compound	Sakura Finetech	Cat#4583
RIPA Buffer (10X)	Cell Signaling Technology	Cat#9806
Experimental models: Cell lines		
Mouse embryonic fibroblasts (MEFs)	Wakabayashi et al., 2009[46]	N/A
Drp1 KO MEFs	Wakabayashi et al., 2009[46]	N/A
HEK293T cells	ATCC	CRL-3216
Experimental models: Organisms/strains		
Mouse: *Drp1 S579D*	This paper	N/A

(*Continued on next page*)

Continued

REAGENT or RESOURCE	SOURCE	IDENTIFIER
Mouse: *Drp1 S579R*	This paper	N/A
Recombinant DNA		
pHR-SIN Drp1 short (Drp1 short isoform; UniProt ID: Q8K1M6-3; 699 aa), see Figure S1A	This paper	N/A
pHR-SIN Drp1 short S579D	This paper	N/A
pHR-SIN Drp1 short S579A	This paper	N/A
pHR-SIN Drp1 BCD (Drp1 isoform with alternative exon B, C, and D; 749 aa), see Figures S1A and S1B	This paper	N/A
pHR-SIN Drp1 CD (Drp1 isoform with alternative exon C and D; 736 aa), see Figures S1A and S1B	This paper	N/A
pHR-CMV8.2ΔR	Stewart et al., 2003[69]	Addgene Plasmid#8455
pCMV-VSVG	Stewart et al., 2003[69]	Addgene Plasmid#8454
Software and algorithms		
ImageJ	NIH	https://imagej.nih.gov/ij/index.html
Prism	GraphPad	https://www.graphpad.com/scientific-software/prism/
ANY-maze	Stoelting	https://www.any-maze.com/

RESOURCE AVAILABILITY

Lead contact

Further information and requests for resources should be directed to and will be fulfilled by the lead contact, Hiromi Sesaki (hsesaki@jhmi.edu).

Materials availability

Mouse and cell lines and plasmids constructed in this study are available from the lead contact upon request.

Data and code availability

- All data reported in this paper will be shared by the lead contact upon request.
- This paper does not report original code.
- Any additional information required to reanalyze the data reported in this paper is available from the lead contact upon request.

EXPERIMENTAL MODEL AND STUDY PARTICIPANT DETAILS

Animals

All experimental work involving animals was conducted in accordance with the guidelines set by the Johns Hopkins University Committee on Animal Care and Use (Protocol number: MO23M109). To create Drp1 S579D and S579R mice using the CRISPR/Cas system, we procured crRNA (5′-UGGCCUUUCUGUGGACUUGCGUUUUAGAGCUAUGCU-3′) and homology-directed repair ssDNA oligonucleotides (5′-AGAATTACTTGCTGAAGAAAAATCAAAACCAATTCCAATTATGCCTGCAGACCCACAGAAAGGCCATGCTGTCAATTTGCTAGATGTGGTAAGCCACCAC-3′) from Integrated DNA Technologies. The targeted gRNA site is depicted in Figures 2A and S1A. A mixture containing Cas9 protein, tracrRNA, crRNA, and ssDNA oligonucleotide in injection buffer (10 mM Tris-HCl, 0.1 mM EDTA) was injected into the pronuclei of zygotes from B6SJLF1/J mice (sourced from Jackson Laboratory; stock#100012) at the Johns Hopkins University Transgenic Facility. The embryos were then cultured at 37°C in a CO_2 incubator for 2 hours before being transferred into the oviducts of pseudopregnant ICR females purchased from Envigo. The genotypes of the resulting pups were determined through DNA sequencing, using the primers 5′-GTCCCATCTGCAGGTGGTGGGATT-3′ and 5′-TAAACAGAATTGTGGTGGCTTACC-3′. The ssDNA oligonucleotides were designed to generate S579D. DNA sequencing revealed that, while some of the mice carry mutations resulting in S579D, others have mutations leading to S579R (Figure 2A). Mice aged from 1.5 weeks to 7 months were used for experiments. Male and female mice were represented approximately equally.

Cells

WT and Drp1-KO MEFs were cultured in IMDM medium supplemented with 10% FBS.[62] HEK293T cells were maintained in DMEM medium supplemented with 10% FBS.

METHOD DETAILS

Lentiviruses

To produce lentiviruses, pHR-SIN plasmids containing each isoform of Drp1 were co-transfected into HEK293T cells along with two additional plasmids, pHR-CMV8.2ΔR and pCMV-VSVG using Lipofectamine 3000 (Invitrogen).[62,69] Two days post-transfection, the medium containing released viruses was collected. These viruses were then rapidly frozen in liquid nitrogen and stored at −80°C for later use. For lentiviral transduction, MEFs were plated at a density of 8×10^4 cells/well in a 6-well plate and allowed to culture for 24 hours. Subsequently, the cells were incubated with the lentivirus in IMDM supplemented with 10% FBS and 7.5 μg/mL polybrene for an additional 24 hours.

Western blotting

Mouse tissues were harvested, rapidly frozen in liquid nitrogen, and then homogenized in RIPA buffer (Cell Signaling Technology, 9806) supplemented with cOmplete Mini Protease Inhibitor (Roche, 11836170001), Phosphatase Inhibitor Cocktail 2 (Sigma-Aldrich, P5726), and Phosphatase Inhibitor Cocktail 3 (Sigma-Aldrich, P0044). Similarly, MEFs were lysed in the same RIPA buffer containing the protease and phosphatase inhibitors. The lysates were then centrifuged at 14,000 × g for 10 minutes, and the supernatants were collected. Protein concentrations in these supernatants were determined using the Bradford method with a Bio-Rad protein assay. Proteins were separated by SDS-PAGE and subsequently transferred onto Immobilon-FL membranes (Millipore). These membranes were blocked with 3% BSA in PBS-T (PBS containing 0.05% Tween-20) at room temperature for 1 hour. Overnight incubation at 4°C with primary antibodies followed, in a solution of 3% BSA/PBS-T. The antibodies used included Drp1 (BD Biosciences, 611113; 1:2,000 dilution), pDrp1 human S616/mouse S579 (Cell Signaling Technology, 3455; 1:1,000 dilution), PDH subunit E2/E3bp (Abcam, ab110333; 1:2,000 dilution), and GAPDH (Thermo Fisher Scientific, MA5-15738; 1:10,000 dilution). The membranes were washed three times in PBS-T and incubated with fluorescently labeled secondary antibodies at a 1:4,000 dilution in 3% BSA/PBS-T at room temperature for 1 hour. After three additional washes in PBS-T, fluorescence signals were detected using a Typhoon laser-scanner platform (Amersham). The band intensity was quantified using NIH ImageJ software.

Immunofluorescence microscopy on mouse tissue sections

Mice were anesthetized via intraperitoneal injection of Avertin and subsequently fixed through cardiac perfusion using ice-cold 4% paraformaldehyde in PBS.[50,70] The tissues were then dissected and further fixed in 4% paraformaldehyde in PBS at 4°C for 2 hours. Afterward, the samples were incubated overnight in PBS containing 30% sucrose at 4°C and subsequently frozen in OCT compound (Sakura Finetek). Frozen sections were cut to a thickness of 7 μm, and antigen retrieval was performed using 1 mM EDTA with microwave heating. Following PBS washes, the sections were blocked and permeabilized with 10% chicken serum and 0.2% Triton X-100 in PBS for 1 hour at room temperature. The sections were then incubated overnight at 4°C with primary antibodies in PBS-T, followed by a 1-hour incubation with fluorescently labeled secondary antibodies in PBS at room temperature. The primary antibodies used included pDrp1 human Ser616/mouse S579 (1:400 dilution), Car8 (Frontier Institute, Car8-Go-Af780; 1:200 dilution), tyrosine hydroxylase (Abcam, ab101853; 1:400 dilution), NeuN (Sigma-Aldrich, MAB377; 1:400 dilution), pHistone H3 (Invitrogen, MA6-15220; 1:400 dilution), Hsp60 (Cell Signaling Technology, 12165; 1:400 dilution), and aconitase 2 (Proteintech, 11134-1-AP; 1:200 dilution). Secondary antibodies, purchased from Invitrogen and used at a 1:200 dilution, included Alexa 488 anti-rabbit IgG (A21206), Alexa 568 anti-goat IgG (A11057), and Alexa 568 anti-mouse IgG (A10037). Imaging was performed using a Zeiss LSM800 GaAsP laser scanning confocal microscope equipped with a 63× objective lens. Image analysis was conducted using NIH ImageJ software.

Immunofluorescence microscopy on MEFs

MEFs were fixed in pre-warmed 4% paraformaldehyde in PBS at room temperature for 20 minutes on an 8-well chambered cover glass.[13,62,71] They were then permeabilized using PBS containing 0.1% Triton X-100 at room temperature for 8 minutes. Following permeabilization, the cells were blocked in 0.5% BSA/PBS at room temperature for 30 minutes. Overnight incubation with primary antibodies in 0.5% BSA/PBS was conducted at 4°C, which was followed by a 1-hour incubation with fluorescently labeled secondary antibodies in PBS at room temperature. The primary antibodies used included pDrp1 S579 (1:200 dilution), pHistone H3 (1:200 dilution), Drp1 (Cell Signaling Technology, 8570; 1:200 dilution) for Figure 4E, Drp1 (BD Biosciences, 611113; 1:200 dilution) for Figure 5C, and TOM20 (Proteintech, 11802-1-AP; 1:300 dilution). The secondary antibodies (Invitrogen), used at a 1:400 dilution, were Alexa 488 anti-rabbit IgG, Alexa 568 anti-mouse IgG, Alexa 488 anti-mouse IgG (A21202), and Alexa 568 anti-Rabbit IgG (A10042). Imaging was performed using a Zeiss LSM800 GaAsP laser scanning confocal microscope with a 63× objective. NIH ImageJ software was used for image analysis.

Behavior analysis

Behavioral tests were conducted on mice aged between 1.5 and 7 months at the Johns Hopkins University School of Medicine's Behavior Core.[15] In the open field test, mice were placed in a Photo-beam Activity System Open Field (San Diego Instruments) for 30 minutes, and their movements were recorded. The chamber, a clear Plexiglas box measuring 45 × 45 cm, was equipped with 16 horizontal photo beams

to measure locomotion and location preferences, assessed by counting beam breaks. During the rotarod tests, mice were placed on a 3.0 cm diameter rod in the Rotamex-5 system (Columbus Instruments). The rod's speed began at 4.0 rpm and increased by 0.6 rpm every 5 seconds. The duration each mouse remained on the rod before falling was noted. This was repeated in three consecutive trials, and the average time for each mouse was calculated. For the elevated plus maze test, mice were positioned in the center of a maze with two open and two closed arms. They were allowed to explore for 5 minutes, with their behavior recorded on video. Entries into both the open and closed arms were tracked using the ANY-Maze Video Tracking System (Stoelting). In the Y-maze spontaneous alternation test, mice were placed at the end of one arm of the maze. They had 5 minutes of free exploration, recorded on video. Spontaneous alternation, defined as consecutive entries into three different arms, was calculated as a percentage using the ANY-Maze Video Tracking System. Lastly, the Y-maze spatial recognition test, divided into training and testing phases with a 30-minute interval, started with one arm blocked during training. Mice were placed at the end of the two open arms for 5 minutes, then returned to their home cage. Post-interval, the block was removed, and during the test phase, mice were placed at the end of a previously open arm and allowed another 5 minutes of exploration. The number of entries into both new and familiar arms was recorded using the ANY-Maze Video Tracking System.

QUANTIFICATION AND STATISTICAL ANALYSIS

Statistical analysis is performed using GraphPad Prism 7 and described in corresponding figure legends.